LINEAR INDUCTION ACCELERATORS AT THE LOS ALAMOS NATIONAL LABORATORY DARHT FACILITY

Subrata Nath
Los Alamos National Laboratory, Los Alamos, NM 87545, USA

Abstract

The Dual-Axis Radiographic Hydrodynamic Test Facility (DARHT) at Los Alamos National Laboratory consists of two linear induction accelerators at right angles to each other. The First Axis, operating since 1999, produces a nominal 20-MeV, 2-kA single beam-pulse with 60-nsec width. In contrast, the DARHT Second Axis, operating since 2008, produces up to four pulses in a variable pulse format by slicing micro-pulses out of a longer ~1.6-microseconds (flat-top) pulse of nominal beam-energy and -current of 17 MeV and 2 kA respectively.

Bremsstrahlung x-rays, shining on a hydro-dynamical experimental device, are produced by focusing the electron beam-pulses onto a high-Z target. Variable pulse-formats allow for adjustment of the pulse-to-pulse doses to record a time sequence of x-ray images of the explosively driven imploding mock device. Herein, we present a sampling of the numerous physics and engineering aspects along with the current status of the fully operational dual axes capability. First successful simultaneous use of both the axes for a hydrodynamic experiment was achieved in 2009.

INTRODUCTION

The Dual Axis Radiographic Hydrodynamic Test (DARHT) facility (Fig.1) was conceived in early 1980's. In the absence of underground nuclear testing, the science, technology and engineering underpinning of stockpile stewardship program - surety, reliability and predictability rests on complex computational and modeling capabilities. DARHT serves as the experimental tool to benchmark and verify the models and computational codes.

DARHT consists of two electron Linear Induction Accelerators (LIA), oriented orthogonally to each other. The two LIAs make the bremsstrahlung radiographic source spots for orthogonal views of each test object. Each generates a high current, 17- to 20-MeV electron beam. Each of the beams converges onto high-Z target producing bremsstrahlung radiation in the form a white spectrum x-rays.

The DARHT Axis I has been operational [1] since 1999 and provides a single high resolution radiograph. The 1st axis accelerator consists of a 4-MV, electron injector delivering a ~2-kA and ~60-ns beam pulse onto a linear string of 64 accelerating induction cells each operating at a nominal voltage of 250-kV.

Axis II LIA was successfully commissioned in 2008. While the 1st axis delivers only a single pulse, the 2nd axis, in contrast, can deliver multiple pulses in a variable format (width) by slicing micro-pulses out of a longer ~1.6μs flat-top pulse of nominal beam-energy and beam-current of ~17 MeV and ~2 kA respectively. The 2nd axis LIA is unique in the world in that its beam pulse has a long, 1.6-μs flattop during which the kinetic energy varies by less than ~1%.

The 2nd axis is an advanced, one-of-a-kind machine and as such inherently more complex. Therefore, the most of the contents of this paper will primarily be focused on the Axis II.

Figure 1: Aerial view of the Dual Axis Radiographic Hydrodynamic Test (DARHT) facility at the Los Alamos National Laboratory.

DARHT ACCELERATORS

The DARHT Axis I and Axis II accelerator-cells occupying the two orthogonal wings of the facility are shown in Figs. 2 and 3. Details of the accelerators are available in publications on DARHT over the last decade. They will be referred to in the relevant sections.

In the first axis, the initial electron beam is formed in a field emission cathode. Ordinary velvet is the material of choice as the cathode surface because of its low emission threshold electric field (< 50 kV/cm). The current density is ~ 100A/cm^2 for the 1st axis cathode [2], typical of a field emission cathode. It is driven by high voltage transmission line ideally suited for short i.e., 60 nsec pulse length. The ferrite-core loaded 64 accelerating cells operating at ~250 kV each, produce a beam of ~20 MeV focused onto a Tantalum x-ray conversion target. The x-ray generating spot size is less than 2.0 mm (50%MTF,

see discussion under downstream transport section) in diameter. The resulting x-ray dose is ~600 Rad at 1-meter.

The layout of the Axis-II LIA, its design and beam characteristics, are described in Ref. [3-6]. The kicker and downstream transport (DST) to the bremsstrahlung converter are described in Ref. [7]. The beam simulation codes used for design of the magnetic focusing tunes are described in Ref. [8-12].

Figure 2: An end-view of the DARHT Axis I accelerator hall showing the linear string of accelerating cells.

The DARHT Axis II accelerator consists of a ~2.5 MeV injector and 6 injector cells each operating at ~175 kV and 68 accelerating cells each operating at ~200 kV delivering a ~17-MeV, ~2-kA beam of 1.6-μsec duration (flat top).

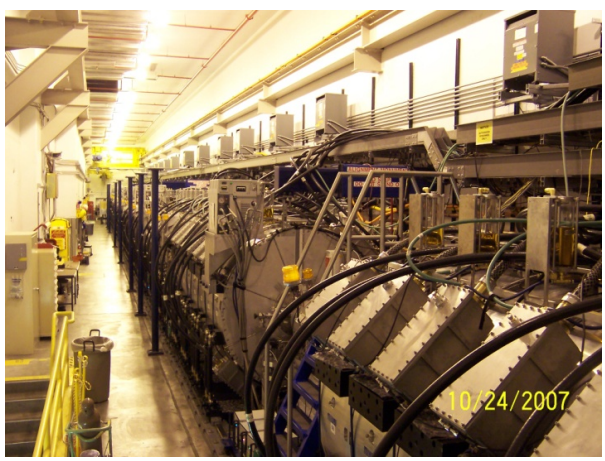

Figure 3: An end-view of the DARHT Axis II accelerator hall showing the linear string of accelerating cells.

The injector cathode is a 6.25" diameter thermionic cathode of 311-XM type (from Spectramat Inc.). The injector is driven directly by a Marx generator. The long-pulse 2-kA beam from the injector can be shortened, when needed, to as little as 200-nsec flat-top pulse with a crowbar switch. Each of the accelerating cells has built-in solenoid to provide the required focusing field for beam transport as well as x- and y-dipoles for beam steering. The accelerator cells are 1.85-m in diameter, weigh 7300 kg each and have a bore of 25.4-cm (35.4 cm for the injector cells to accommodate larger beam diameter near the injector). The high-voltage vacuum insulator is made of mycalex. The magnetic material in the form of annular metglass cores are located in the oil volume and provide 480-520mV-sec capacity. Each cell is driven by a tunable pulse forming network (PFN) unit.

A downstream transport section (DST) that follows the accelerator section, transports the beam to the x-ray conversion target. The default setting is to transport the entire long beam pulse to a Graphite-Tungsten beam dump aided by a set of magnetic elements - dipoles and quadrupole. A multi-pulse electromagnetic kicker in the DST diverts selected slices of the long main pulse to the x-ray conversion target while the un-kicked portions of the beam follow the default trajectory to the dump.

Table 1, below shows comparative capabilities of the two axes of DARHT for one of many possible operational formats.

Table 1: Parameters for Axis I and Axis II in One of Many Possible Formats

Parameter (Nominal Values)	**DARHT Axis I**	**DARHT Axis II**
Beam Energy (MeV)	20	17
Beam Current (kA)	1.9	1.8
Injector Energy (MeV)	4	2.5
Number of Cells @kV (Loaded)	64@250	8@180 66@200
Pulse length (Flat-top)	60 ns	1.6μs
Number of Pulses	1	4
X-Ray Pulse Length Range (nsec)	60	25 - 65
Dose at 1 meter (Rad)	580	100, 190, 250, 260
Spot Size in mm (50% MTF)	1.7	1.9, 1.7, 2.0, 2.4

OPERATIONAL RESULTS

In what follows, we will discuss aspects of beam physics through the accelerator and the DST in Axis II, which as noted earlier, is challenging due to unusually long and high beam current of the pulse from the Axis II injector.

Non-interceptive beam diagnostics, such as beam position monitors (BPMs), are used for tuning as well as routine operation [5, 6]. BPMs are located throughout the injector, accelerator, and DST. BPMs separated by ~5 m in the accelerator measure current and position, while the BPMs in the DST have the eight detectors required to provide ellipticity measurements [5, 13]. Interceptive diagnostics are only occasionally used. Magnetic spectrometer to measure beam-electron kinetic energy,

and time-resolved imaging of the beam current profile using Cerenkov emitters [4-7, 14] during commissioning are examples of such diagnostics. The kinetic energy of the accelerated beam is around 17 MeV for more than 1.6 μs, the exact value of which depends on the operating cell- and injector-voltage. For a given established tune, the beam is very reproducible. The day-to-day variation of beam position at the exit is less than 0.5 mm, which is about 10% of the beam radius predicted by the envelope codes.

In Axis II, we have successfully addressed the most vexing physics issues generic to the high-current electron linacs. They have been reported in detail in Ref. [15]. A short discussion follows.

High-Frequency Motion – BBU

High-frequency beam motion, with period less than the FWHM of the kicked pulse, increases the source spot size.

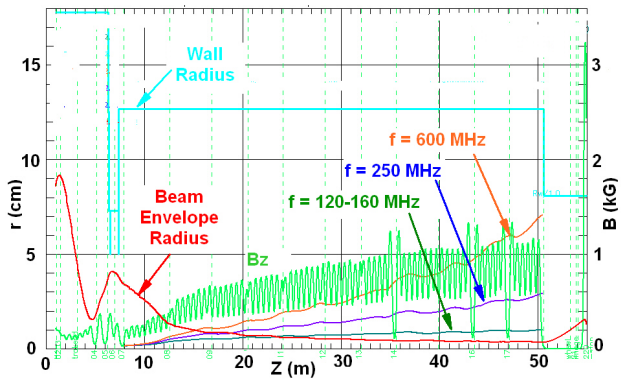

Figure 4: Beam envelope simulation for the accelerator tune. Also shown is the saturated growth of the three principal modes of BBU for a 50-micron initial perturbation. Growth is shown as a percentage of beam radius (left scale). The locations of BPMs are shown as vertical green dotted lines.

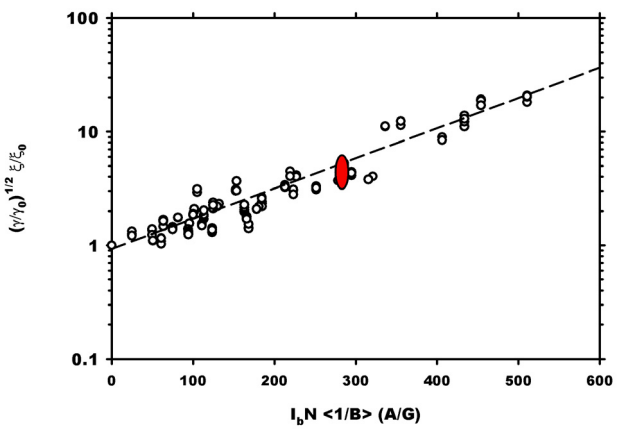

Figure 5: BBU growth. Open circles: data obtained in 1.3-kA experiments with an early 50-cell configuration of the Axis II LIA [6]. Filled (red) oval: range of data obtained during 1.8-kA experiments with the present full energy configuration.

Since the Axis-II cells have TM mode resonances higher than 100 MHz, large-amplitude beam breakup instability (BBU) would pose a problem. Corrective measures were taken to suppress this instability both through the design of the cells and through the tuning of the accelerator focusing fields.

The Axis-II LIA accelerating cells incorporate ferrite tiles to reduce the cell transverse impedance by damping the TM modes responsible for the BBU. As an additional step, we use tunes that incorporate very strong solenoidal focusing fields. Detail discussion of the BBU and confirmation of theoretical predictions was detailed in Ref. [6]. Tunes have been developed with magnetic fields strong enough to suppress the BBU to an amplitude < 10% of beam radius (Fig. 4).

As described in Ref. [6], we performed extensive BBU experiments with an early configuration of the Axis-II LIA to confirm the theoretical predictions of saturated growth for the high-current, strongly-focused regime. The observed BBU in the present full energy configuration agrees with those measurements, and with the theory, as shown in Fig. 5.

Low-Frequency Motion – Beam Sweep

Low frequency beam motion results in the transverse displacement of the centers of successive x-ray source spots. Left uncorrected, beam motion at the exit of the Axis-II LIA is dominated by an energy dependent sweep, with > 5 mm amplitude over the 1.6-μs flattop. Since this implies displacement of the x-ray source spots by more than their size, it must be corrected.

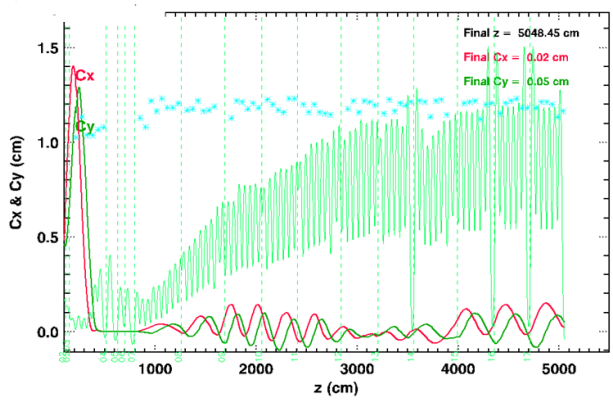

Figure 6: Beam centroid position in x (Cx in red) and y (Cy in green). For this simulation, the initial offset and resulting large helical motion has been corrected and the beam centered. The residual helical motion is the result of cell misalignments.

The source of this sweep is the interaction of the beam with random dipoles introduced by small misalignments (~ 25-μm rms offset, ~0.3-mr rms tilt) of cells. Any tilt of the beam trajectory resulting from interaction with a dipole field will cause the beam to follow a helical trajectory through the remaining solenoids, with a gyro-radius and phase that depends on the beam energy. Since there is a dipole field in the injector diode (because of the asymmetric current paths), this helix is initially large, but

can be corrected using steering dipoles in the injector cells (Fig. 6). However, even after correcting this initial offset, the beam takes up a helical trajectory due to the misalignment induced random dipoles.

For constant beam energy, this helix is stationary, but if the energy varies, the phase at the LIA exit varies, causing the position to sweep in time. In realty, there is a time variation (see Fig. 7) of the kinetic energy at the LIA exit due largely to the pulsed-power driving the accelerating cells.

Suppression of this energy-dependent motion by using steering dipoles in a procedure known as a "tuning V" was demonstrated on other LIAs [16]. Significant reduction in the sweep amplitude in Axis II has been achieved using only a few of the available steering dipoles. This issue and results after successful corrections are described in detail by Ekdahl et al. in Ref. [15].

Beam Transport to Downstream Section

Downstream transport section elements, the beam properties therein and the beam spot size has been described in detail in an earlier paper [7].

As noted in Ref. [7], the kicker can be programmed to kick up to four pulses spaced over the span of the flattop; the pulse lengths can be varied anywhere between 20 to 250 nsec depending on the experimental need. Locations of the four sliced pulses spanning over the full length of the flat top are shown in Fig. 7. Average energy of the kicked beam pulses varies by less than ± 0.25%. An example of the resulting four pulses with current of ~1.8 kA spanning over the ~1.6 µsec flattop is shown in Fig. 8.

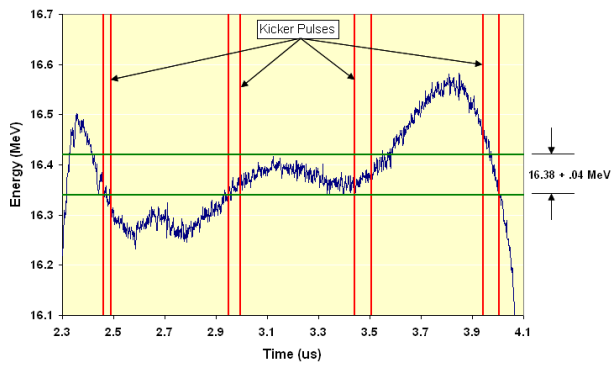

Figure 7: Location of the four beam slices over the span of the flat top. Note the suppressed-zero energy scale.

Since the completion of the full energy commissioning of Axis II in 2008 [7], significant improvements have been made in the beam-optics through the accelerator and the downstream transport section resulting in improved x-ray source spot sizes and the dose. Fig. 9 highlights the progressive improvement in the spot size. The largest improvement is on the 2nd pulse, 55% and least improved one is the 4th pulse, as expected, which had a modest improvement of 34%. The dose is measured with diamond radiation detectors (DRDs) located downstream of the x-ray conversion target. Table 2 shows the pulse length, and the resulting dose in a recently conducted experiment. The source spot size numbers in Fig. 9 are full width half maximum (FWHM) values. In imaging community, an accepted practice is to use 50% MTF, modulation transfer function. The 50% MTF spot size is the diameter of a uniformly illuminated disc with the same MTF half-width as the measured intensity distribution. A useful rule of thumb is that for a Gaussian distribution, the 50% MTF spot size is ~1.6 times FWHM [17].

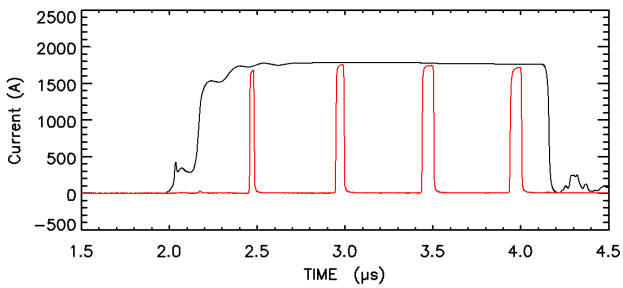

Figure 8: Overlay of current at accelerator exit (black) and after the kicker (red) showing the long accelerated-current pulse and four kicked-beam pulses.

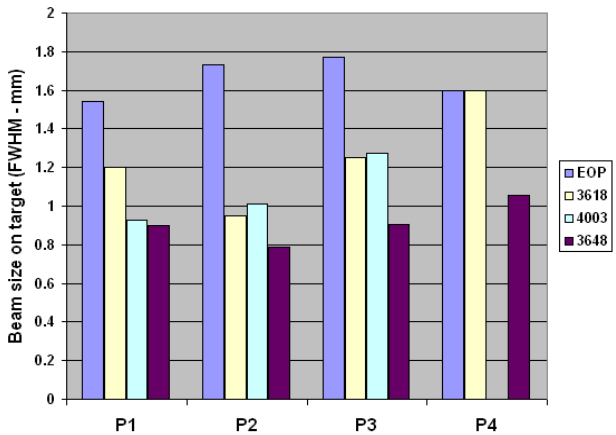

Figure 9: Beam-spot sizes at the x-ray production target for tunes used in the recently conducted experiments and at the end of the (full energy commissioning) project, EOP.

Table 2: Pulse Format and Dose for a Recently Conducted Experiment

Pulse	Pulse length (ns)	Dose at 1 m (R)	Dose Rate (R/ns)
P1	23.5	102	4.34
P2	46.0	190	4.13
P3	64.5	253	3.92
P4	64.0	260	4.06

Figure 10 shows the spot sizes on the x-ray conversion target of a recently conducted experiment. The spot sizes shown are 50% MTF values.

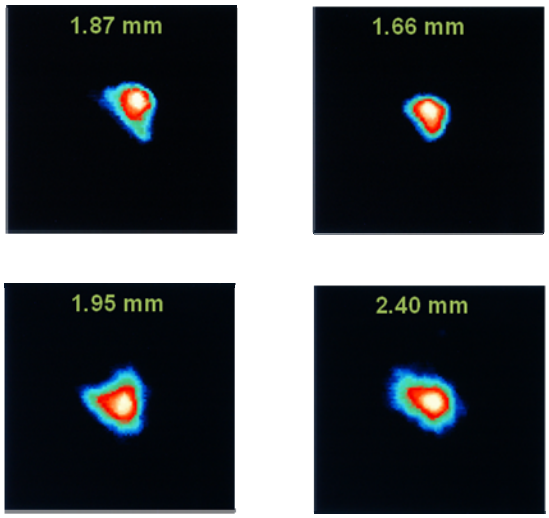

Figure 10: Source-spots for four pulses on the x-ray conversion target in a recent experiment. The noted numbers for the size are 50% MTF values.

SUMMARY

Since the completion of full energy commissioning in 2008, DARHT Axis II has transitioned to reliable operation providing unprecedented data for radiographic experiments. Up to four pulses are being successfully transported to the x-ray production target with significantly improved beam spot-size. Beam motion from several sources is understood, well controlled and can be further improved, if needed. On a concluding note, operational reliability of DARHT Axis II has seen a notable and measurable improvement as it transitioned from commissioning to operation, achieved principally through operation at slightly lower voltages.

ACKNOWLEDGEMENTS

Successful transition of the DARHT Axis II from commissioning to sustained operation leading to a series of successful hydro-experiments could not have been possible but for the dedicated effort by the entire DARHT team members, past and present. Special thanks to J. Barraza, C. Ekdahl, M. Schulze, J. Seitz and K. Nielsen for their tireless efforts towards a successfully operating machine and to C. Ekdahl and M. Schulze for help with this manuscript.

This work was supported by the US National Nuclear Security Agency and the US Department of Energy under contract W-7405-ENG-36.

REFERENCES

[1] M. J. Burns et al., "Status of the DARHT Phase 2 Long-Pulse Accelerator," in Proc. 2001 Particle Accel. Conf., (2001), pp. 325-329.

[2] H. Davis and R. D. Scarpetti, "Modern Electron Induction Linacs," in Proc. 2006 Int. LINAC Conf., (2006), pp. 208-212 and references cited therein.

[3] R. D. Scarpetti et al., "Status of the DARHT 2nd Axis Accelerator at the Los Alamos National Laboratory," in Proc. 2007 Part. Accel. Conf., (2007), pp. 831-835.

[4] Carl Ekdahl, et al., "First beam at DARHT-II," in Proc. 2003 Part. Accel. Conf., (2003), pp. 558-562.

[5] Carl Ekdahl, et al., "Initial electron-beam results from the DARHT-II linear induction accelerator," IEEE Trans. Plasma Sci. 33, (2005), pp. 892-900.

[6] Carl Ekdahl, et al., "Long-pulse beam stability experiments on the DARHT-II linear induction accelerator," IEEE Trans. Plasma Sci. 34, (2006), pp.460-466.

[7] Martin Schulze, et al., "Commissioning the DARHT-II Accelerator Downstream Transport and Target," in Proc. 2008 Linear Accel. Conf., (2008), pp. 427-429.

[8] T. P. Hughes, David C. Moir and Paul W. Allison, "Beam injector and transport calculations for ITS," in Proc. 1995 Part. Accel. Conf., (1995), pp. 1207-1209.

[9] T. P. Hughes, et al., "LAMDA User's Manual and Reference", Voss Scientific technical report VSL-0707, April 2007.

[10] E. P. Lee and R. K. Cooper, "General envelope equation for cylindrically symmetric charged-particle beams," Part. Acc. 7, (1976), pp. 83-95.

[11] S. Humphries Jr., "TRAK – Charged particle tracking in electric and magnetic fields," in Computational Accelerator Physics, R. Ryne Ed., New York: American Institute of Physics, (1994), pp. 597-601.

[12] T. P. Hughes, R. E. Clark, and S. S. Yu, "Three-dimensional calculations for a 4 kA, 3.5 MV, 2 microsecond injector with asymmetric power feed," Phys. Rev. ST AB 2, (1999), pp. 110401:1 – 6.

[13] Carl Ekdahl, "Aliasing errors in measurements of beam position and ellipticity," Rev. Sci. Instrum. 76, (2005), pp. 095108:1 –9.

[14] H. Bender, et al., "Quasi-anamorphic optical imaging system with tomographic reconstruction for electron beam imaging," Rev. Sci. Instrum. 78, (2007), pp. 013301.

[15] C. Ekdahl et al., "Beam Dynamics in a Long-Pulse Linear Induction Accelerator," to be presented in EAPPC-BEAMS2010, Jeju, S. Korea, 2010, and references cited therein.

[16] J. T. Weir, et al., "Improved ETA-II accelerator performance," in Proc. 1999 Particle Accelerator Conf., (1999), pp. 3513-3515.

[17] C. Ekdahl, "Modern Electron Accelerators for Radiography," IEEE Transactions on Plasma Sc., vol. 30, No. 1, Feb. 2002, pp. 254-261.